Optics and Lasers in Engineering 102 (2018) 100–105

Contents lists available at ScienceDirect

Optics and Lasers in Engineering

journal homepage: www.elsevier.com/locate/optlaseng

Polarization-multiplexing ghost imaging

Shi Dongfeng[a,d], Zhang Jiamin[a,b], Huang Jian[a,b,*], Wang Yingjian[a,b], Yuan Kee[a], Cao Kaifa[c], Xie Chenbo[a], Liu Dong[a], Zhu Wenyue[a]

[a] Key Laboratory of Atmospheric Optics, Anhui Institute of Optics and Fine Mechanics, Chinese Academy of Sciences, Hefei 230031, China
[b] University of Science and Technology of China, Hefei 230026, China
[c] School of Environment and Energy Engineering, Anhui Jianzhu University, Hefei 230601, China
[d] Key Laboratory of Optical Engineering, Chinese Academy of Sciences, Chengdu 610209, China

ARTICLE INFO

Keywords:
Polarization-multiplexing
Ghost imaging

ABSTRACT

A novel technique for polarization-multiplexing ghost imaging is proposed to simultaneously obtain multiple polarimetric information by a single detector. Here, polarization-division multiplexing speckles are employed for object illumination. The light reflected from the objects is detected by a single-pixel detector. An iterative reconstruction method is used to restore the fused image containing the different polarimetric information by using the weighted sum of the multiplexed speckles based on the correlation coefficients obtained from the detected intensities. Next, clear images of the different polarimetric information are recovered by demultiplexing the fused image. The results clearly demonstrate that the proposed method is effective.

1. Introduction

Ghost imaging (GI) [1–9] employs a non-spatially resolving detector, called as single-pixel detector, to acquire the image of objects. In conventional GI systems, the light is split into two beams using a beam splitter to obtain two correlated light speckles. One beam, which illuminates the objects, is collected by a non-spatially resolving detector, while the other beam is recorded by a spatially resolving detector, e.g., a charge-coupled device (CCD) camera. The signals from the spatially resolving detector do not contain information of the objects. However, the image of the objects can be recovered by calculating the correlation between the signals from the two detectors. Computational GI [1–5] uses a computer controlled spatial light modulator (SLM) that replaces the beam splitter and spatially resolving detector. Thus, only a non-spatially resolving detector, such as a photomultiplier tube or an avalanche photodiode, is employed as the imaging device in the computational GI system, where there is no scanning device. This new imaging system, which includes an integrated computational algorithm, can reduce the cost or size of the matrix detectors, especially in the infrared and terahertz regions of the spectrum [2,3], where the matrix detectors do not show as good performance as in the visible spectrum. In a weak light environment, the GI system can also be used to obtain image with higher signal-to-noise ratio (SNR) than that recorded by matrix detectors [6].

Polarization [10] is an intrinsic feature of light that provides valuable information of objects beyond that provided by their spectral and intensity distributions. Polarization seeks to measure information of the vector nature of the optical field across a scene. Depolarization is defined as the process of changing polarized light into unpolarized light and reducing the degree of polarization. In fact, when an optical beam interacts with objects, its polarization state almost always changes; the objects of different materials exhibit different depolarization characteristics. Therefore, the light reflected (or transmitted) from the objects encoded by the degree of polarization can be employed to distinguish objects made of different materials. It is well known that a promising method for improving the ability of imaging system identification is to employ the polarization components of the reflected light from objects. Thus far, polarimetric imaging with matrix detectors [11–14] has been widely studied and applied in several domains, such as machine vision, biomedical imaging and remote sensing. The influence of light polarization on visibility and SNR in GI systems has been investigated [15]. The theoretical analysis shows that the visibility of the image of no-depolarization object increases with the increasing degree of thermal light polarization.

The connection between polarization and GI can improve the performance of GI in several domains, such as machine vision, biomedical imaging, and remote sensing. In polarimetric GI (PGI) [16–19] systems, the reflective intensity of objects is decomposed into different polarization intensities. Computational PGI systems [17,18] with multiple

* Corresponding author at: Key Laboratory of Atmospheric Optics, Anhui Institute of Optics and Fine Mechanics, Chinese Academy of Sciences, Hefei 230031, China
E-mail addresses: dfshi@aiofm.ac.cn (S. Dongfeng), jhuang@aiofm.ac.cn (H. Jian).

https://doi.org/10.1016/j.optlaseng.2017.10.022
Received 18 August 2017; Received in revised form 17 October 2017; Accepted 26 October 2017
Available online 6 November 2017
0143-8166/

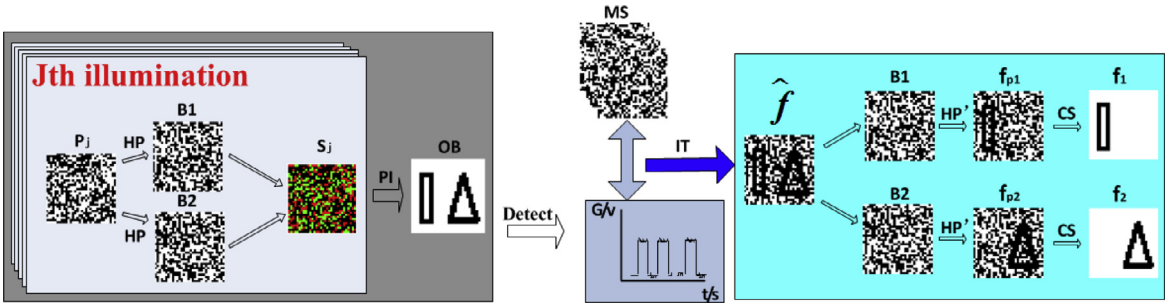

Fig. 1. Procedure of the proposed method: MS: multiplexed speckles, P_j: jth multiplexed speckle; B1 and B2: two complementary binary encoded matrices; S_j: jth illumination speckle where different colors represent different polarization states; HP: Hadamard product of P_j and the encoded matrices; PI: projection illumination; OB: objects; G: intensities detected by the single-pixel detector; IT: iterative reconstruction method; HP': Hadamard product of the fused information $\hat{f}$ and the encoded matrices; f_{p1} and f_{p2}: two random partial polarimetric sampling images; CS: compressed sensing algorithm that is used to compute images of different polarimetric information; f_1 and f_2: two recovered polarimetric images. (For interpretation of the references to color in this figure legend, the reader is referred to the web version of this article).

photodetectors have been proposed to simultaneously obtain images of different linear polarization states. For some data acquisition systems, the maximum sampling rate in the multi-channel acquisition mode is lower than that in the single channel acquisition mode. For example, the maximum sampling rate of the data acquisition system in the single channel acquisition mode, which is used in the reference [4], is 5 GSs^{-1}. However, when a two-channel acquisition mode of the data acquisition system is employed in the experiment, the maximum sampling rate becomes 2.5 GSs^{-1}, and the depth resolution of the imaging system for 3D imaging is reduced. For other data acquisition systems, the maximum sampling rate does not change in different acquisition modes; the amount of acquired data will be large and this will result in a higher demand for data storage, transmission, and processing of the imaging system. These problems will become more pronounced when PGI with multiple photodetectors is utilized for 3D imaging using the time-of-flight method because the system needs high-speed acquisition of the echo signal. It is also possible to use a single detector to obtain different polarization states in a time-sharing manner [19], but this method does not apply in real-time situations. In order to address these problems, we employ spatial polarization multiplexing in this paper to simultaneously acquire multiple polarimetric information by a single detector, which is unlike previous studies on PGI. It does not reduce the maximum sampling rate and imaging efficiency of the system. In the remainder of this paper, we describe the method employed in the study and present the results.

2. Theoretical analysis

The theory of this method will now be introduced. The Stokes vector S [10], which consists of four parameters $(I, Q, U, V)^T$, is employed to describe the polarization state. Here, I represents the total intensity of the light, Q is the difference between the horizontal and vertical polarizations, U is the difference between the linear + 45° and –45° polarizations, and V is the difference between the right and left circular polarizations. The degree of polarization is a quantity used to describe the portion of an electromagnetic wave that is polarimetric. The polarization state of the reflected light from the objects changes relative to that of the incident light. The relationship between the incident light S_{in} and reflected light S_{re} is given by the following equation:

$$S_{re}(x, y) = M(x, y)S_{in}(x, y), \tag{1}$$

where $M(x,y)$ is the Mueller matrix of the object surface. For light retroreflected off nonbirefringent materials, the Mueller matrix can be approximated as [12,13]

$$M(x, y) = \begin{pmatrix} m_{00}(x, y) & 0 & 0 & 0 \\ 0 & m_{11}(x, y) & 0 & 0 \\ 0 & 0 & m_{11}(x, y) & 0 \\ 0 & 0 & 0 & m_{33}(x, y) \end{pmatrix}, \tag{2}$$

where m_{00} is the reflective coefficient of the objects, and m_{11} and m_{33} are the linear and circular depolarization parameters of the objects, respectively.

Based on Eqs. (1) and (2), we can obtain the reflected light $S_{re}(x,y) = (m_{00}(x,y)^*I(x,y),\ m_{11}(x,y)^*Q(x,y),\ m_{11}(x,y)^*U(x,y),\ m_{33}(x,y)^*V(x,y))^T$, whose polarization state can be controlled by the incident light $S_{in}(x,y) = (I(x,y),\ Q(x,y),\ U(x,y),\ V(x,y))^T$. Rotating polarizers or multi-detectors are often used to obtain the full Stokes vector $S_{re}(x,y)$. It will be either a slow and storage-heavy task or a complex imaging system. In order to address this problem, the first two components of the Stokes parameters instead of all the Stokes parameters are measured; this can also describe well the polarization characteristics of the objects [14]. Existing research methods on PGI [16–19] use multiple detectors or time-difference acquisition to obtain different polarimetric information and recover the object information. In contrast, in this paper, the spatial polarization multiplexing method is employed to acquire multiple polarimetric information simultaneously by using a single detector. Multiple polarimetric information can be recovered from a single measurement, which significantly reduces the data acquisition or/and allows fast data communication to users. Therefore, the system efficiency can be greatly increased using the proposed method compared with the prior literatures concerning PGI methods [17–19].

The whole procedure of the proposed technique is illustrated in Fig. 1, in which two different polarized objects serve as an example. First, the computer program produces two complementary binary-encoded matrices (B1, B2) and multiplexed speckles (MS). Here, we design the optical path such that the two complementary binary-encoded matrices represent two different polarization states. The illumination speckles S are produced by fusing the matrices obtained by multiplying the multiplexed speckles and encoded matrices. The assembly procedure of the illumination speckle S_j is shown in the gray frame of Fig. 1. This process can be described by Eq. (3). The illumination speckles are projected onto the objects, and this process is denoted by the symbol PI. The reflected light from the two objects passes a polarizer and is detected by a single-pixel detector. The detected intensities are denoted by the symbol G. The fused image of the two polarized objects can be restored using an iterative reconstruction (IT) method, which can be expressed as a weighted sum of the multiplexed speckles (MS) based on the corresponding coefficients obtained from the detected intensities. The mathematical representation is described by Eq. (12). Next, two

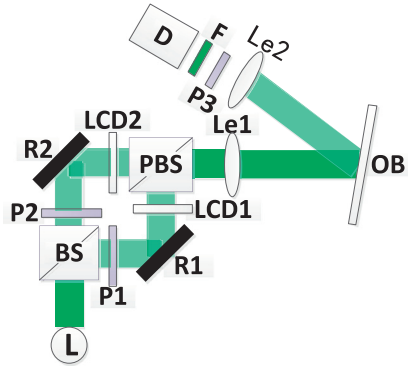

Fig. 2. Configuration of the GI system based on polarization-division multiplexing speckles. L: light source; BS: beam splitter; PBS: polarization beam splitter; P1 and P3: horizontal polarizers; P2: vertical polarizer; R1 and R2: reflected mirrors; OB: objects; Le1 and Le2: lenses; F: filter; D: single-pixel detector; LCD1 and LCD2: liquid crystal displays.

random sampling images, f_{p1} and f_{p2}, indicating different random partial polarimetric information, can be recovered by multiplying the fused image and encoded matrices (B1, B2), respectively. This process is defined by Eqs. (13) and (14). Finally, the final images of the two sets of different polarimetric information can be obtained using the compressed sensing (CS) algorithm, respectively. This process can be expressed as Eq. (15). The CS theory [20] allows the recording an image consisting of N^2 pixels using much fewer than N^2 measurements if it can be transformed to a basis where most pixels have negligibly small values. For example, theoretically, a 1 mega-pixel array could potentially be used to reconstruct a 4 mega-pixel image. Specifically, a random sample of the 4 mega-pixel image is taken and then recovered through sparse signal reconstruction methods. This is possible because natural images tend to be sparse (i.e., only a small fraction of these projections have relevant information) in some bases of functions. The hardware limitations of traditional imaging systems in terms of their spatial resolution and temporal resolution can be effectively addressed using this characteristic. To date, several matrix imaging systems [21–23] have been built, and the effectiveness of the theory has been confirmed experimentally. For example, a method of efficient space-time sampling with pixel-wise coded exposure to reconstruct a video from a single coded image while maintaining high spatial resolution has been proposed [21]. Additionally, Liang et al. have accomplished single-shot compressed ultrafast photography at one hundred billion frames per second with random sampling [22]. Collecting the spectral information of an imaging scene via random sampling has also been proposed [23].

Our experimental setup is sketched in Fig. 2. A 532 nm continuous wave (cw) laser serves as the light source. Light is split into two beams by a beam splitter (BS). One beam passes through the polarizer P1 and becomes horizontal light; it is reflected by R1, modulated by the liquid crystal display (LCD1), and then finally enters the polarization beam splitter (PBS). The modulated information of LCD1 can be expressed as the Hadamard product of P_j and the binary-encoded matrix B1. The other beam passes through the polarizer P2 and becomes vertical light; it is reflected by R2, modulated by the liquid crystal display (LCD2), and then finally enters the polarization beam splitter (PBS). The modulated information of LCD2 can be expressed as the Hadamard product of P_j and the binary-encoded matrix B2. Polarization-division multiplexing speckles combined by the PBS illuminate the objects. The reflected intensity from the objects (OB) passes through a lens (Le2), linear horizontal polarizer (P3), and filter (F) with center wavelength 532 nm, which is employed to filter out background stray light, and then is detected by a single-pixel detector (D).

Assuming that the objects are sampled at the jth time using the multiplexed speckle P_j, the polarization-division multiplexing speckle has vertical and horizontal polarization states, which is used to illuminate the objects. According to the above analysis, the Stokes vectors of the polarization-division multiplexing speckle can be written as

$$\begin{aligned} S_{in}(x,y) &= P_j(x,y)B_1(x,y)(1\ \ 1\ \ 0\ \ 0)^T + P_j(x,y)B_2(x,y)(1\ \ -1\ \ 0\ \ 0)^T \\ &= P_j(x,y)(B_1(x,y)+B_2(x,y)\ \ B_1(x,y)-B_2(x,y)\ \ 0\ \ 0)^T \end{aligned} \tag{3}$$

where the first and second terms are the binary light distributions with different polarizations modulated by the two polarizers and LCDs, respectively. Suppose two binary-encoded matrices have the following properties:

$$B_{i1}(x,y)B_{i2}(x,y) = \begin{cases} 0 & i1 \neq i2 \\ B_{i1}(x,y) & i1 = i2 \end{cases}, \tag{4}$$

$$\prod B_i = E, \tag{5}$$

where E represents a matrix with all entries are equal to 1, and $\prod$ indicates the accumulation of all matrices. The reflected light from the objects can be expressed as

$$S_{re}(x,y) = P_j(x,y)\begin{pmatrix} m_{00}(x,y)(B_1(x,y)+B_2(x,y)) \\ m_{11}(x,y)(B_1(x,y)-B_2(x,y)) \\ 0 \\ 0 \end{pmatrix}. \tag{6}$$

In front of the detector, a linear horizontal polarizer (P3) is employed to obtain the linearly polarized reflected light intensities. The Mueller matrix of the linear horizontal polarizer can be expressed as [10]

$$M_{\parallel} = \frac{1}{2}\begin{bmatrix} 1 & 1 & 0 & 0 \\ 1 & 1 & 0 & 0 \\ 0 & 0 & 0 & 0 \\ 0 & 0 & 0 & 0 \end{bmatrix}. \tag{7}$$

Based on Eqs. (1), (6) and (7), the detected intensity from the single-pixel detector can be written as

$$\begin{aligned} g_j &= \frac{1}{2}\sum P_j(x,y)m_{00}(x,y)(B_1(x,y)+B_2(x,y)) \\ &\quad + \frac{1}{2}\sum P_j(x,y)m_{11}(x,y)(B_1(x,y)-B_2(x,y)). \end{aligned} \tag{8}$$

On further simplifying Eq. (8), we have

$$g_j = \sum\nolimits_{x,y} P_j(x,y)\hat{f}(x,y). \tag{9}$$

where

$$\hat{f}(x,y) = \frac{1}{2}m_{00}(x,y)(B_1(x,y)+B_2(x,y)) + \frac{1}{2}m_{11}(x,y)(B_1(x,y)-B_2(x,y)), \tag{10}$$

where the fused image $\hat{f}(x,y)$ represents the accumulation of the random samples from multiple polarimetric information. From Eq. (9), we can determine that the acquisition process can be described by the interaction between the multiplexed speckles and the fused image. Various patterns of speckles can be used in this system. Random patterns, in which each pixel has random gray values, can be employed. But it needs a great number of measurements and long time for imaging by correlation algorithm [5]. In this case, CS can also be employed to reduce the total number of illumination speckles, but CS algorithm has some shortcomings that it may take much more time than that in the calculation of correlation. And the time consumed increases exponentially with the data volume which is directly related to the size of the image to be recovered [7]. In practice, CS algorithms are very difficult to implement for large image with high pixel count, or may even fail to work under specific circumstances [8]. Hadamard and Fourier patterns provide another strategy that enables the reconstruction of the image with a linearly iterative algorithm, which requires very low computational complexity. Fourier patterns are more efficient than Hadamard patterns while Hadamard patterns are more noise-robust than Fourier patterns. When image quality and accuracy are concerned, the Hadamard patterns are the primary selection [9]. Thus, multiplexed speckles with

Hadamard patterns are used in this study. As the illumination speckles produced by the LCD system are binary, we create complementary pairs of illumination speckles H_+ and H_- to indirectly access the Hadamard patterns. The intensities detected when the illumination speckles H_{j+} and H_{j-} are used to illuminate the objects can be expressed as g_{j+} and g_{j-}, respectively; then, the two intensities are subtracted. This process can be written as

$$\begin{aligned} g_j &= g_{j+} - g_{j-} \\ &= \sum\nolimits_{N\times N} \left(H_{j+}(x,y) - H_{j-}(x,y)\right)\hat{f}(x,y) \\ &= \sum\nolimits_{N\times N} P_j(x,y)\hat{f}(x,y), \end{aligned} \tag{11}$$

The iterative reconstruction method [4] is employed to recover the fused object information, which can be expressed as

$$\hat{f}(x,y) = \sum P_j(x,y)g_j, \tag{12}$$

where $\hat{f}(x,y)$ is the recovered fusion image. Here, the number of multiplexed speckles is equal to j. The above formula indicates that the fused image can be expressed as a weighted sum of the multiplexed speckles based on the corresponding coefficients obtained from the detected intensities. The above equation also demonstrates that when the reflected intensities of different polarizations are detected, they are mixed together. Thus, the image containing multiple polarizations is recovered by the iterative reconstruction method. However, we must obtain the image for each set of polarimetric information. Based on the properties of the encoded matrices, the random samples of each polarization can be obtained as follows:

$$\hat{f}_{p1} = B_1(x,y)\hat{f}(x,y) = [m_{00}(x,y) + m_{11}(x,y)]B_1(x,y)/2, \tag{13}$$

$$\hat{f}_{p2} = B_2(x,y)\hat{f}(x,y) = [m_{00}(x,y) - m_{11}(x,y)]B_2(x,y)/2. \tag{14}$$

From the above formula, the Hadamard product of the fused image and the encoded matrices can be used to obtain the corresponding random polarimetric information. Based on the polarization character of the encoded matrices, f_{p1} and f_{p2} are defined as the horizontal and vertical polarizations, respectively. Next, the complete information of each polarization can be determined with high precision by substituting the encoded matrices and the random sampled image in the CS algorithm. Optimization can be achieved as follows:

$$f_{pi} = \varphi a_{pi} \text{ subject to } \min\left\{\left\|\hat{f}_{pi} - B_{pi}\varphi a_{pi}\right\|^2 + \gamma T(a_{pi})\right\}, \tag{15}$$

Here, φ represents the transformation of the chosen domain resulting in a sparse representation a_i, and γ and T represent the regularization coefficient and function, respectively. The code employed for CS in this paper [24] is the function *Inpainting_GSR* of the software package. When the encoded matrices are unknown, the accurate object information cannot be obtained. Accordingly, the encoded matrices of the proposed method used as keys can result in the encryption of the polarization information. According to the information obtained from the two directions of polarization, the intensity and linear polarimetric information can be achieved as:

$$f_I = f_{p1} + f_{p2} = m_{00}(x,y), \tag{16}$$

$$f_P = \frac{\left|f_{p1} - f_{p2}\right|}{f_{p1} + f_{p2} + \varepsilon} = \frac{m_{11}(x,y)}{m_{00}(x,y) + \varepsilon}, \tag{17}$$

where ε is a constant that prevents a division by zero. Next, we will introduce the experimental results.

3. Experimental verification

The left image in Fig. 3 shows the experimental scene with two piglets. The top and bottom piglets are composed of aluminum and plastic, respectively. The polarization parameters m_{00} and m_{11} between objects composed of aluminum and plastic are very different, so the results

Fig. 3. Experimental illustration: on the left are the objects, and on the center and right are the encoded matrices. The encoded matrices are 128×128 binary matrices, which contain 8192 elements equal to 1 and where different colors represent different polarization states. The compression ratio is 50%.

can be conveniently used to analyze the system performance. The middle and right images in Fig. 3 represent two polarization complementary binary-encoded matrices, where the different polarization states are represented in different colors. The resolution of the 0.79 inch LCDs is 1024×768 pixels. In the experiments, the central 256×256 pixels of the LCDs with a 2×2 binning model is employed, making the resolution of the object image as 128×128. A Thorlabs PMT-PMM02 is used as the single-pixel detector. The correlation coefficients between the under-sampled images and a reference image are employed to compare the recovered images. This coefficient ranges from zero to one, depending on the resemblance of both images. Our reference image is always the image acquired without under-sampling. The correlation coefficient is calculated with the following function:

$$r = \frac{\sum_{m,n}(A_{mn} - \bar{A})(B_{mn} - \bar{B})}{\sqrt{\sum_{m,n}(A_{mn} - \bar{A})^2(B_{mn} - \bar{B})^2}}, \tag{18}$$

where A and B are the image matrices with indices m and n, respectively, and $\bar{A}$ and $\bar{B}$ represent the mean values of the elements in A and B.

The evolutionary linear iterative method [4] is employed to recover the fused images in the experiment. The evolutionary linear iteration scheme chooses a subset of Hadamard speckles to recover the fused image of the multiple objects by selecting the patterns with the most significant intensities measured by the single-pixel detector. The recovered fusion images based on the intensities of the reflected light are shown in Fig. 4, and each image presents the results obtained using different numbers of multiplexed speckles. The results show that the qualities of the recovered images increase as the number of multiplexed speckles increase. However, we cannot identify the multi-polarization information from the results in Fig. 4. Fortunately, based on the properties of the encoded matrices, two images of different polarizations can be obtained by multiplying the fused image with the encoded matrices, as shown in the first and third rows of Fig. 5. Finally, the results of the final recovered images of the horizontal and vertical polarizations obtained using the CS algorithm are shown in the second and fourth rows of Fig. 5. The experiment was determined to be successful based on the fact that completely accurate image information could be recovered exactly from the compressed samples via the CS algorithm. The correlation coefficients of the horizontal and vertical polarizations with the reference information are 0.942, 0.964, 0.989, 0.998 and 0.909, 0.948, 0.988, 0.977 in compression ratios of 12.5%, 25%, 50%s and 75%, respectively. The results indicate that the quality of the recovered images is affected by the quality of the fused image and that a positive correlation exists between them. The differences among the images reconstructed from the fused images with the coverage spanning compression ratios ranging from 50% to 100% are almost negligible. According to the results, the different encoded matrices could effectively achieve the fusion of multi-polarization information. The compression ratio of the encoded matrices is 50%, so the fusion of two sets of polarimetric information is achieved. If the compression ratio is further reduced, the images corresponding to additional polarimetric information can be fused and imaged using the results of one measurement. Compared with the traditional PGI systems,

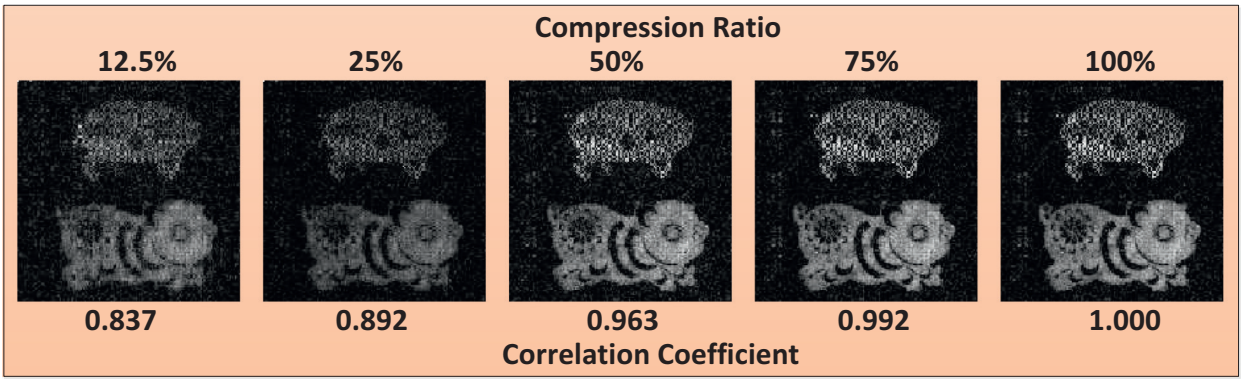

Fig. 4. Fused image reconstruction with different compression ratios. The correlation coefficients between the recovered images with different compression ratios and the reconstruction utilizing a complete Hadamard basis (100% compression ratio) are shown.

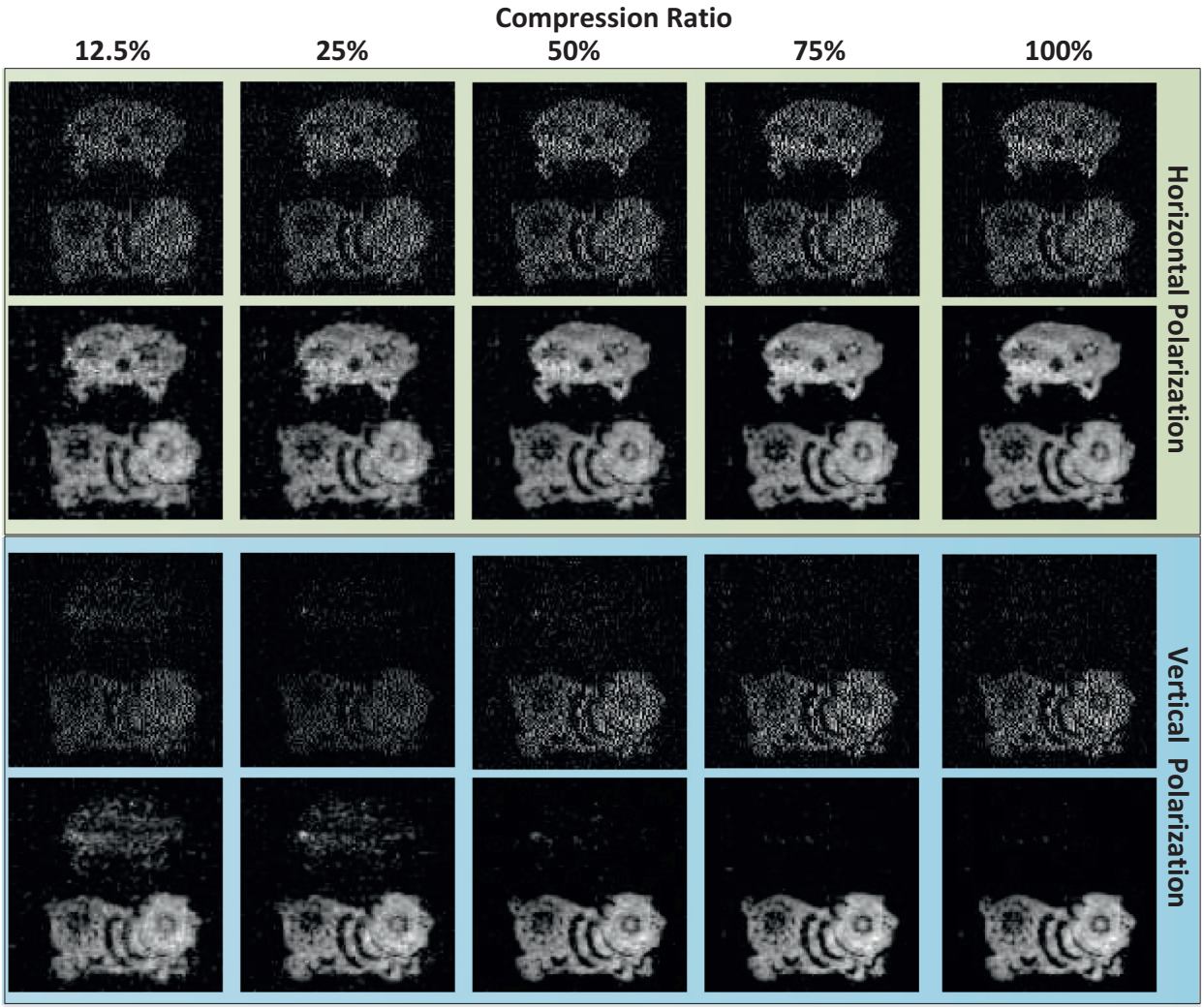

Fig. 5. Multiple polarimetric information reconstructed with different compression ratios using reflected light. The first and third rows present the compressed images obtained by multiplying the fusion result with the encoded matrices, and the second and fourth rows present the final recovered results of the horizontal and vertical polarization.

where each of the different polarization states must be individually measured, the proposed method can effectively reduce the data acquisition and improve the imaging efficiency.

According to the recovered results of Fig. 5, the corresponding intensity and polarimetric images can be obtained according to Eqs. (16) and (17), and the results are presented in Fig. 6. The first row gives the intensity images obtained at different compression ratios and the second row presents the corresponding linear polarimetric images. The results are based on the fact that the depolarization of the metal object is less than that of the plastic object. According to the results shown in the figure, we can use our method to achieve the classification of the different polarized objects.

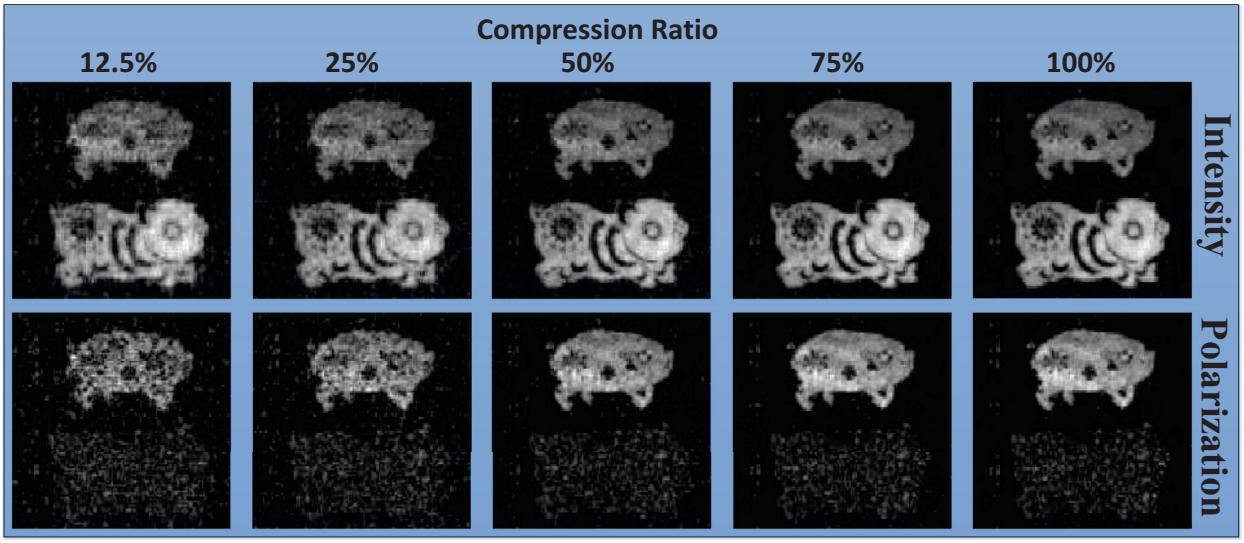

Fig. 6. Recovered results. The first row presents the intensity images with different compression ratios. The second row presents the polarimetric images with different compression ratios.

4. Summary

In this paper, we first propose polarization-multiplexing GI technique, which was described by theoretical analysis and experiments. Unlike previous studies, we employed spatial polarization multiplexing to acquire multiple polarimetric information simultaneously by a single detector. In the experiments, the application of this system to the detection of two objects made of different materials was presented. It was clearly demonstrated that the proposed method is effective. Of course, a single detector can be employed to obtain more polarimetric information simultaneously by extending this method. For example, three sets of polarimetric information can be achieved simultaneously by a single detector by improving the current maturity of the 3LCD or 3DMD systems. Furthermore, the polarimetric micro-mirror array can be used to directly perform polarization multiplexing modulation of the beam. In general, the central challenge addressed by this method is to find an architecture that effectively balances the final recovery image quality with the number and pattern of the encoded matrices. The choice of an encoded matrix plays a key role in image reconstruction. Because various matrices can be chosen, the problem of optimizing the encoded matrix should be carefully studied in the future. Further studies could also involve the sensitivity of the technique to the detection noise, the effects of rough surfaces, the sensitivity of more than two different materials, and its performance under atmospheric turbulence.

Acknowledgments

This work was supported by the National Natural Science Foundation of China (Nos. 11404344, 41505019 and 41475001), the CAS Innovation Fund Project (No. CXJJ-17S029) and Open Research Fund of Key Laboratory of Optical Engineering, Chinese Academy of Sciences(No. 2017LBC007).

References

[1] Shapiro JH, Boyd RW. The physics of ghost imaging. Q Inf Process 2012;11:949–93.
[2] Aspden RS, Gemmell NR, Morris PA, Tasca DS, Mertens L, Tanner MG, et al. Photon-sparse microscopy: visible light imaging using infrared illumination. Optica 2015;2:1049–52.
[3] Stantchev RI, Sun B, Hornett SM, Hobson PA, Gibson GM, Padgett MJ, et al. Noninvasive, near-field terahertz imaging of hidden objects using a single-pixel detector. Sci Adv 2016;2:e1600190.
[4] Sun MJ, Edgar MP, Gibson GM, Sun BQ, Radwell N, Lamb R, et al. Single-pixel three-dimensional imaging with time-based depth resolution. Nat Commun 2016;7.
[5] Sun B, Edgar MP, Bowman R, Vittert LE, Welsh S, Bowman A, et al. 3D computational imaging with single-pixel detectors. Science 2013;340:844–7. doi:10.1126/science.1234454.
[6] Morris PA, Aspden RS, Bell JEC, Boyd RW, Padgett MJ. Imaging with a small number of photons. Nat Commun 2015;6 doi:Artn 591310.1038/Ncomms6913.
[7] Averbuch A, Dekel S, Deutsch S. Adaptive compressed image sensing using dictionaries. Siam J Imag Sci 2012;5:57–89. doi:10.1137/110820579.
[8] Yu WK. Adaptive compressive ghost imaging based on wavelet trees and sparse representation. Opt Express 2014;22:7133–44. doi:10.1364/Oe.22.007133.
[9] Zhang Z, Wang X, Zheng G, Zhong J. Hadamard single-pixel imaging versus Fourier single-pixel imaging. Opt Express 2017;25(16):19619–39.
[10] Brosseau C. Fundamentals of polarimetric light: a statistical optics approach. John Wiley; 1998.
[11] Tyo JS, Goldstein DL, Chenault DB, Shaw JA. Review of passive imaging polarimetry for remote sensing applications. Appl Opt 2006;45:5453–69.
[12] Chun CSL, Sadjadi FA. Polarimetric laser radar target classification. Opt Lett 2005;30:1806.
[13] b Breugnot S, Cle´menceau P. Modeling and performances of a polarization active imager at λ=. Opt Eng 2000;39:2681.
[14] Laurenzis M, Lutz Y, Christnacher F, Matwyschuk A, Poyet J-M. Homogeneous and speckle-free laser illumination for range-gated imaging and active polarimetry. Opt Eng 2012;51:061302.
[15] Shirai T, Kellock H, Setälä T, Friberg AT. Visibility in ghost imaging with classical partially polarimetric electromagnetic beams. Opt Lett 2011;36:2880–2.
[16] Shi D, Hu S, Wang Y. Polarimetric ghost imaging. Opt Lett 2014;39:1231–4.
[17] Stephen SWelsh, Edgar MatthewP, Bowman Richard, Sun Baoqing, Padgett MilesJ. Near video-rate linear Stokes imaging with single-pixel detectors. J Opt 2015;17(2):025705.
[18] Liu YX, Shi JH, Zeng GH. Single-photon-counting polarization ghost imaging. Appl Opt 2016;55:10347–51.
[19] Shi DF, Wang F, Jian H, Cao KF, Yuan KE, Hu SX, et al. Compressed polarimetric ghost imaging of different material's reflective objects. Opt Rev 2015;22(6):882–7.
[20] Candes EJ, Wakin MB. An introduction to compressive sampling. IEEE Signal Process Mag 2008;25:21–30. doi:10.1109/Msp.2007.914731.
[21] Hitomi Y, Gu JW, Gupta M, Mitsunaga T, Nayar SK. Video from a single coded exposure photograph using a learned over-complete dictionary. In: 2011 IEEE international conference on computer vision (ICCV); 2011. p. 287–94.
[22] Gao L, Liang JY, Li CY, Wang LHV. Single-shot compressed ultrafast photography at one hundred billion frames per second. Nature 2014;516**74**-U159. doi:10.1038/nature14005.
[23] Lin X, Wetzstein G, Liu YB, Dai QH. Dual-coded compressive hyperspectral imaging. Opt Lett 2014;39:2044–7. doi:10.1364/Ol.39.002044.
[24] Zhang J, Zhao DB, Gao W. Group-based sparse representation for image restoration. IEEE T Image Process 2014;23:3336–51.